State feedback control in equinoctial variables for orbit phasing applications

(Article begins on next page)

05 May 2024

State Feedback Control in Equinoctial Variables for Orbit Phasing Applications

Mirko Leomanni[*], Gianni Bianchini[†], Andrea Garulli [‡], Antonio Giannitrapani [§]

Università di Siena, Siena, 53100, Italy

I.   Introduction

Orbit phasing operations play an important role in many space missions, being commonly performed for station acquisition and station keeping of Low-Earth-Orbit and Geostationary satellites, and in the initial part of rendezvous maneuvers. The classical phasing approach consists of two-impulse Hohmann transfer which takes a satellite away from and then back into its original orbit, so as to steer the satellite to the correct orbital position, see, e.g., [1]. This control method is flight-proven, conceptually simple, and fuel-efficient in most applications, but suffers from two major limitations: it is inherently open-loop, and requires an impulsive thrust approximation. Due to the tight positioning accuracy requirements of next-generation space missions and the availability of new continuous-thrust propulsion technologies [2,3], there is a growing interest in the development of feedback control systems able to overcome such limitations.

To this aim, the orbit phasing problem can be treated as a rendezvous problem between two satellites located at different angular positions within an orbit. As long as the satellite relative distance is small compared to the orbit radius, standard linearized models such as the Hill-Clohessy-Wiltshire (HCW) [4] and Tschauner-Hempel (TH) [5] equations can be adopted for control design. Along this line, references [6–8] developed optimal and robust regulators solving the circular rendezvous problem. Model Predictive Control has been investigated in [9–11] to deal with state and

---

[*]Research associate, Department of Information Engineering and Mathematics, `leomanni@diism.unisi.it`
[†]Professor, Department of Information Engineering and Mathematics, `giannibi@diism.unisi.it`
[‡]Professor, Department of Information Engineering and Mathematics, `garulli@diism.unisi.it`
[§]Professor, Department of Information Engineering and Mathematics, `giannitrapani@diism.unisi.it`

input constraints. References [12–17] extended these results to the case of elliptical orbits.

The design of feedback regulators able to handle large inter-satellite separations, such as those typically encountered during phasing operations, has received comparatively less attention. Lyapunov-based nonlinear stabilization methods have been investigated in [18–21]. These methods provide analytical control laws, but, in general, do not minimize a predefined maneuver cost. Optimal solutions based on nonlinear model predictive control and receding-horizon strategies, see, e.g., [22–24], have also been considered. These techniques are usually computationally intensive, as they require to solve a nonlinear optimization problem at each time step.

As suggested in [25], the above difficulties can be alleviated by casting the phasing problem in a curvilinear coordinate system, and performing linearization in such coordinates. Nevertheless, this approach is still limited by the assumption of a small relative radius, which is generally not met for elliptical formations. In this note, we relax this assumption by introducing a specific orbital-element-based parametrization of the relative dynamics, inspired by that in [26–28]. In particular, the formulation in [28] is suitably modified to include the effect of a nonconservative control acceleration. Moreover, the adopted parametrization allows one to streamline the control design problem. The resulting linearized model accounts for arbitrarily large relative phase errors and orbital eccentricities and, in this respect, extends the classical derivations.

The proposed formulation is exploited for the synthesis of two state-feedback controllers: a time-invariant Linear Quadratic Regulator (LQR) for circular phasing maneuvers and a periodic LQR for elliptical ones. The performance of these controllers is evaluated through numerical simulations on the full nonlinear model describing the orbital motion. It is observed that the control objective can be achieved successfully despite the presence of a large initial phase error. Moreover, the simulations show that, by applying the standard LQR methodology to the proposed model, one can suitably trade off the control effort and the tracking performance. This is particularly relevant for space missions involving low-thrust propulsion.

The note is organized as follows. In Section II, the equinoctial form of Gauss' Variational Equations is recalled. Section III introduces the key coordinate change which leads to the derivation of the linearized model describing the relative motion. The LQR design problem is formulated

by using these new model in Section IV. The applicability of the proposed design is investigated through numerical simulations in Section V, and some final considerations are drawn in Section VI.

II. Mathematical Background

Let S^1 and $\mathbb{R}^n$ denote the unit circle and the n-dimensional Euclidean space, respectively. In this note, the motion of a satellite in a closed orbit is described in terms of the equinoctial variables $\mathbf{x} = [x_1 \ \ldots \ x_6]^T \in S^1 \times \mathbb{R}^5$, defined as follows

$$
\begin{aligned}
x_1 &= \Omega + \omega + \theta \\
x_2 &= \sqrt{\mu/a^3} \\
x_3 &= e\cos(\Omega + \omega) \\
x_4 &= e\sin(\Omega + \omega) \\
x_5 &= \tan(i/2)\cos(\Omega) \\
x_6 &= \tan(i/2)\sin(\Omega),
\end{aligned}
\tag{1}
$$

where x_1 is the true longitude, x_2 is the mean motion, (x_3, x_4) are the components of the eccentricity vector, and (x_5, x_6) are the components of the inclination vector, being $a, e, i, \Omega, \omega, \theta$ the classical orbital elements (semi-major axis, eccentricity, inclination, longitude of the ascending node, argument of periapsis, true anomaly) and μ the gravitational parameter. The parametrization (1) describes the satellite motion with respect to a given right-handed inertial coordinate frame $\mathcal{F}$ centered at the Earth. For the sake of clarity, we introduce the following auxiliary quantities

$$
\begin{aligned}
w &= \sqrt{1 - x_3^2 - x_4^2} \\
[\ \zeta_3 \ \ \zeta_4 \ ]^T &= \Psi(x_1)[\ x_3 \ \ x_4 \ ]^T \\
[\ \zeta_5 \ \ \zeta_6 \ ]^T &= \Psi(x_1)[\ x_5 \ \ x_6 \ ]^T,
\end{aligned}
\tag{2}
$$

where $\Psi(x_1)$ denotes the reflection matrix

$$
\Psi(x_1) = \begin{bmatrix} \cos(x_1) & \sin(x_1) \\ \sin(x_1) & -\cos(x_1) \end{bmatrix}.
\tag{3}
$$

The satellite dynamics can be modeled by the input-affine nonlinear system

$$\dot{\mathbf{x}} = \mathbf{f}(\mathbf{x}) + \mathbf{g}(\mathbf{x})\mathbf{u}, \tag{4}$$

where the vector fields $\mathbf{f}(\mathbf{x})$ and $\mathbf{g}(\mathbf{x})$ are specified by the Gauss' Variational Equations ([29], Chapter 10), as follows

$$\mathbf{f}(\mathbf{x}) = \left[\begin{array}{cc} \dfrac{(1+\zeta_3)^2}{w^3}x_2 & 0_{1\times 5} \end{array} \right]^T, \tag{5}$$

$$\mathbf{g}(\mathbf{x}) = \frac{w}{(\mu\, x_2)^{1/3}} \begin{bmatrix} 0 & 0 & \dfrac{\zeta_6}{1+\zeta_3} \\[2mm] -\dfrac{3\zeta_4}{w^2}x_2 & -\dfrac{3(1+\zeta_3)}{w^2}x_2 & 0 \\[2mm] \sin(x_1) & \dfrac{x_3+(2+\zeta_3)\cos(x_1)}{1+\zeta_3} & -\dfrac{\zeta_6}{1+\zeta_3}x_4 \\[2mm] -\cos(x_1) & \dfrac{x_4+(2+\zeta_3)\sin(x_1)}{1+\zeta_3} & \dfrac{\zeta_6}{1+\zeta_3}x_3 \\[2mm] 0 & 0 & \dfrac{1+x_5^2+x_6^2}{2(1+\zeta_3)}\cos(x_1) \\[2mm] 0 & 0 & \dfrac{1+x_5^2+x_6^2}{2(1+\zeta_3)}\sin(x_1) \end{bmatrix}, \tag{6}$$

and $\mathbf{u} = [u_1\ u_2\ u_3]^T$. The inputs u_1, u_2 and u_3 denote the radial, tangential and normal components of a perturbing acceleration, expressed in the Radial-Transverse-Normal (RTN) frame centered at the satellite.

For the purpose of our work, it is worth introducing the mean longitude $L = L(x_1, x_3, x_4)$, defined by the equinoctial form of Kepler's equation

$$L = \Gamma - x_3 \sin(\Gamma) + x_4 \cos(\Gamma), \tag{7}$$

where $\Gamma = \Gamma(x_1, x_3, x_4)$ is the so-called eccentric longitude. The time derivative of (7) can be expressed as [29]

$$\dot{L} = x_2 + \mathbf{h}(\mathbf{x})\mathbf{u}, \tag{8}$$

where

$$\mathbf{h}(\mathbf{x}) = \frac{w}{(\mu x_2)^{1/3}} \left[\frac{-\zeta_3}{1 + w} + \frac{-2w}{1 + \zeta_3} \quad \frac{(2 + \zeta_3)\zeta_4}{(1 + w)(1 + \zeta_3)} \quad \frac{\zeta_6}{1 + \zeta_3} \right]. \tag{9}$$

It is well-known that x_1 in (1) can be uniquely computed as a function of L, x_3, and x_4, although not in closed form. Hereafter, this implicit function will be denoted by $x_1 = \chi(L, x_3, x_4)$.

In the next section, a new dynamic model is developed, describing the relative motion between two satellites in terms of the considered equinoctial variables.

III.   Relative Motion Dynamics

In this section, we consider a controlled chaser satellite and an uncontrolled target satellite. The chaser dynamics are given by (4), where $\mathbf{u}$ is treated as a control input. The trajectory of the target satellite is described by the reference vector

$$\mathbf{x}^*(t) = [x_1^*(t) \ x_2^* \ x_3^* \ x_4^* \ x_5^* \ x_6^*]^T, \tag{10}$$

where $x_2^*, \ldots, x_6^*$ are constant parameters, and $\mathbf{x}^*(t)$ satisfies the orbital equation

$$\dot{\mathbf{x}}^* = \mathbf{f}(\mathbf{x}^*), \tag{11}$$

corresponding to (4) with $\mathbf{u} = \mathbf{0}$.

We find it convenient to parameterize the motion of the chaser relative to the target in terms of the error vector $\boldsymbol{\xi} = [\xi_1 \ldots \xi_6]^T \in S^1 \times \mathbb{R}^5$, defined as follows

$$
\begin{aligned}
\xi_1 &= L - L^* \\[4pt]
\xi_2 &= \frac{x_2}{x_2^*} - 1 \\[4pt]
\begin{bmatrix} \xi_3 \\ \xi_4 \end{bmatrix} &= \boldsymbol{\Psi}(x_1) \begin{bmatrix} x_3 - x_3^* \\ x_4 - x_4^* \end{bmatrix} \\[4pt]
\begin{bmatrix} \xi_5 \\ \xi_6 \end{bmatrix} &= \boldsymbol{\Psi}(x_1) \begin{bmatrix} x_5 - x_5^* \\ x_6 - x_6^* \end{bmatrix},
\end{aligned} \tag{12}
$$

where $L^* = L(x_1^*, x_3^*, x_4^*)$, and $\Psi(x_1)$ is defined in (3). Notice that $\xi = 0$ if and only if $x = x^*$.

Consider the following time and input scalings

$$d\lambda = x_2^* \, dt \tag{13}$$

$$v = \frac{w^*}{x_2^* (\mu \, x_2^*)^{1/3}} \, u, \tag{14}$$

where $w^* = \sqrt{1 - (x_3^*)^2 - (x_4^*)^2}$ and $v = [v_1, v_2, v_3]^T$. The variable λ will play the role of the integration variable in the error dynamics derived hereafter. By differentiating the smooth mapping (12), taking into account equations (4)-(6), (8)-(9), (11), and applying the scalings (13)-(14), one has that the dynamics of the error is described by

$$\frac{d\xi}{d\lambda} = F(L^*, \xi)\xi + G(L^*, \xi) \, v, \tag{15}$$

where

$$F(L^*, \xi) = \begin{bmatrix} 0 & 1 & 0 & 0 & 0 & 0 \\ 0 & 0 & 0 & 0 & 0 & 0 \\ 0 & 0 & 0 & \dfrac{(1 + \zeta_3)^2 x_2}{-w^3 x_2^*} & 0 & 0 \\ 0 & 0 & \dfrac{(1 + \zeta_3)^2 x_2}{w^3 x_2^*} & 0 & 0 & 0 \\ 0 & 0 & 0 & 0 & 0 & \dfrac{(1 + \zeta_3)^2 x_2}{-w^3 x_2^*} \\ 0 & 0 & 0 & 0 & \dfrac{(1 + \zeta_3)^2 x_2}{w^3 x_2^*} & 0 \end{bmatrix} \tag{16}$$

$$\mathbf{G}(L^*, \boldsymbol{\xi}) = \frac{w\,(x_2^*)^{1/3}}{w^*(x_2)^{1/3}} \begin{bmatrix} \dfrac{-\zeta_3}{1+w} + \dfrac{-2w}{1+\zeta_3} & \dfrac{(2+\zeta_3)\zeta_4}{(1+w)(1+\zeta_3)} & \dfrac{\zeta_6}{1+\zeta_3} \\[2ex] -\dfrac{3\zeta_4 x_2}{w^2 x_2^*} & -\dfrac{3(1+\zeta_3)x_2}{w^2 x_2^*} & 0 \\[2ex] 0 & 2 & \dfrac{(\zeta_4-\xi_4)\zeta_6}{1+\zeta_3} \\[2ex] 1 & \dfrac{\zeta_4}{1+\zeta_3} & \dfrac{(\xi_3-\zeta_3)\zeta_6}{1+\zeta_3} \\[2ex] 0 & 0 & \dfrac{1+\zeta_5^2+\zeta_6^2-2\xi_6\zeta_6}{2(1+\zeta_3)} \\[2ex] 0 & 0 & \dfrac{\xi_5\,\zeta_6}{1+\zeta_3} \end{bmatrix}. \tag{17}$$

Remark 1. *In the matrices* (16)-(17), *the quantities x_2, w, and $\zeta_3, \ldots, \zeta_6$ can be expressed in terms of the error variables $\boldsymbol{\xi}$, the target mean longitude L^* and the constant parameters $x_2^*, \ldots, x_6^*$, by using* (2), (12) *and the fact that $x_1 = \chi(L, x_3, x_4)$. For notational simplicity, the dependence on the constant parameters $x_2^*, \ldots, x_6^*$ is not made explicit in the argument of F and G.*

For any scalar ϕ, the state $\bar{\boldsymbol{\xi}} = [\phi \ 0 \ldots 0]^T$ is an equilibrium for the nonlinear time-varying system (15) with $\mathbf{v} = \mathbf{0}$. Linearizing (15) about $\boldsymbol{\xi} = \bar{\boldsymbol{\xi}}$ and $\mathbf{v} = \mathbf{0}$, one obtains the linearized dynamics

$$\frac{d\boldsymbol{\xi}}{d\lambda} = \mathbf{F}(L^*, \bar{\boldsymbol{\xi}})\bar{\boldsymbol{\xi}} + \left.\frac{\partial[\mathbf{F}(L^*, \boldsymbol{\xi})\boldsymbol{\xi}]}{\partial\boldsymbol{\xi}}\right|_{\boldsymbol{\xi}=\bar{\boldsymbol{\xi}}}(\boldsymbol{\xi} - \bar{\boldsymbol{\xi}}) + \left.\frac{\partial[\mathbf{G}(L^*, \boldsymbol{\xi})\mathbf{v}]}{\partial\mathbf{v}}\right|_{\boldsymbol{\xi}=\bar{\boldsymbol{\xi}}}\mathbf{v}$$

$$= \left\{\mathbf{F}(L^*, \boldsymbol{\xi}) + \left[\frac{\partial F(L^*, \boldsymbol{\xi})}{\partial\xi_1}\boldsymbol{\xi} \ \ldots \ \frac{\partial F(L^*, \boldsymbol{\xi})}{\partial\xi_6}\boldsymbol{\xi}\right]\right\}_{\boldsymbol{\xi}=\bar{\boldsymbol{\xi}}} \boldsymbol{\xi} + \mathbf{G}(L^*, \bar{\boldsymbol{\xi}})\mathbf{v} \tag{18}$$

$$= \mathbf{F}(L^*, \bar{\boldsymbol{\xi}})\boldsymbol{\xi} + \mathbf{G}(L^*, \bar{\boldsymbol{\xi}})\mathbf{v} = \mathbf{F}(L^* + \phi, \mathbf{0})\boldsymbol{\xi} + \mathbf{G}(L^* + \phi, \mathbf{0})\mathbf{v}.$$

In the derivation of (18), the relationships $\mathbf{F}(L^*, \bar{\boldsymbol{\xi}})\bar{\boldsymbol{\xi}} = \mathbf{0}$, $\frac{\partial[\mathbf{F}(L^*, \boldsymbol{\xi})\boldsymbol{\xi}]}{\partial\boldsymbol{\xi}}\bar{\boldsymbol{\xi}} = \mathbf{0}$ and $\frac{\partial\mathbf{F}(L^*, \boldsymbol{\xi})}{\partial\xi_j}\bar{\boldsymbol{\xi}} = \mathbf{0}$ have been exploited. Moreover, we used the fact that L^* and ξ_1 enter in (16)-(17) as $L = \xi_1 + L^*$, see Remark 1, so that $\mathbf{F}(L^*, \bar{\boldsymbol{\xi}})$ and $\mathbf{G}(L^*, \bar{\boldsymbol{\xi}})$ can be equivalently replaced by $\mathbf{F}(L^* + \phi, \mathbf{0})$ and $\mathbf{G}(L^* + \phi, \mathbf{0})$, respectively.

Let the fundamental plane of frame $\mathcal{F}$ be coplanar with the target orbital plane (see Appendix A), and observe that $x_5^* = x_6^* = 0$ with respect to $\mathcal{F}$. Moreover, notice that, being $\dot{L}^* = x_2^*$ from (8) and $\dot{\phi} = 0$, one can set

$$\lambda = L^* + \phi, \tag{19}$$

which is consistent with (13). By using these arguments, we can finally rewrite (18) as

$$\frac{d\boldsymbol{\xi}}{d\lambda} = \mathbf{A}(\lambda)\boldsymbol{\xi} + \mathbf{B}(\lambda)\,\mathbf{v}, \tag{20}$$

where

$$\mathbf{A}(\lambda) = \begin{bmatrix} 0 & 1 & 0 & 0 & 0 & 0 \\ 0 & 0 & 0 & 0 & 0 & 0 \\ 0 & 0 & 0 & \dfrac{(1+\psi_3)^2}{-(w^*)^3} & 0 & 0 \\ 0 & 0 & \dfrac{(1+\psi_3)^2}{(w^*)^3} & 0 & 0 & 0 \\ 0 & 0 & 0 & 0 & 0 & \dfrac{(1+\psi_3)^2}{-(w^*)^3} \\ 0 & 0 & 0 & 0 & \dfrac{(1+\psi_3)^2}{(w^*)^3} & 0 \end{bmatrix} \tag{21}$$

$$\mathbf{B}(\lambda) = \begin{bmatrix} \dfrac{-\psi_3}{1+w^*}+\dfrac{-2w^*}{1+\psi_3} & \dfrac{(2+\psi_3)\psi_4}{(1+w^*)(1+\psi_3)} & 0 \\[2ex] -\dfrac{3\psi_4}{(w^*)^2} & -\dfrac{3(1+\psi_3)}{(w^*)^2} & 0 \\[2ex] 0 & 2 & 0 \\[2ex] 1 & \dfrac{\psi_4}{1+\psi_3} & 0 \\[2ex] 0 & 0 & \dfrac{1}{2(1+\psi_3)} \\[2ex] 0 & 0 & 0 \end{bmatrix}, \tag{22}$$

$$\psi_3 = x_3^* \cos(\chi^*(\lambda)) + x_4^* \sin(\chi^*(\lambda))$$
$$\psi_4 = x_3^* \sin(\chi^*(\lambda)) - x_4^* \cos(\chi^*(\lambda)), \tag{23}$$

and $\chi^*(\cdot) = \chi(\cdot, x_3^*, x_4^*)$ denotes the mapping from the mean longitude to the corresponding true longitude, along the target orbit. The entries in (21)-(22) are obtained from (2) and (16)-(17) by enforcing $x_1 = \chi^*(\lambda)$ and $x_j = x_j^*$, $j = 2, \ldots, 6$, with $x_5^* = x_6^* = 0$.

For the special case of circular reference orbits, featuring $\psi_3 = \psi_4 = 0$ and $w^* = 1$, system (20)

reduces to the linear time-invariant (LTI) system

$$\frac{d\boldsymbol{\xi}}{d\lambda} = \mathbf{A}\,\boldsymbol{\xi} + \mathbf{B}\,\mathbf{v}, \tag{24}$$

where

$$\mathbf{A} = \begin{bmatrix} 0 & 1 & 0 & 0 & 0 & 0 \\ 0 & 0 & 0 & 0 & 0 & 0 \\ 0 & 0 & 0 & -1 & 0 & 0 \\ 0 & 0 & 1 & 0 & 0 & 0 \\ 0 & 0 & 0 & 0 & 0 & -1 \\ 0 & 0 & 0 & 0 & 1 & 0 \end{bmatrix}, \qquad \mathbf{B} = \begin{bmatrix} -2 & 0 & 0 \\ 0 & -3 & 0 \\ 0 & 2 & 0 \\ 1 & 0 & 0 \\ 0 & 0 & 1/2 \\ 0 & 0 & 0 \end{bmatrix}. \tag{25}$$

Note that the left multiplication by $\boldsymbol{\Psi}(x_1)$ in (12) is instrumental to make the control input matrix $\mathbf{B}$ in (25) independent of λ (and hence independent of ϕ).

Remark 2. *Classical linearized models assume the chaser to lie in a local neighborhood of the target (this implies $\phi = 0$ in (18)). The use of the parametrization (12) relaxes this assumption, by allowing one to consider a generic nonzero ϕ, i.e., an arbitrary phase error along the reference orbit. This is the key feature that will be exploited for control design.*

In the following, we investigate the application of linear control design techniques to systems (20) and (24). To this purpose, the domain of definition of the angular variable ξ_1 is restricted to $(-\pi, \pi] \in \mathbb{R}$.

IV.   Control Synthesis

In this section, the linearized models derived in the previous section are used to design state-feedback controllers tailored to orbit phasing applications. In these applications, the chaser satellite moves along an orbit similar to the one of the target (possibly with a very large initial phase offset), and must be steered towards the target position. More specifically, we aim at finding a state-feedback control law

$$\mathbf{v} = -\mathbf{K}\,\boldsymbol{\xi} \tag{26}$$

such that

$$\lim_{\lambda \to \infty} \boldsymbol{\xi}(\lambda) = \mathbf{0}, \tag{27}$$

for a set of initial conditions in a local neighborhood of the target orbit. Two solutions to this problem are presented below, for circular and elliptical orbits. The proposed solutions are based on classical LQR techniques in order to suitably trade-off the control effort and the tracking performance.

A. Circular Case

We consider the circular orbit case first. By using the linear time-invariant model (24), the control design problem is cast as

$$\begin{aligned} \min_{\mathbf{v}} \quad & \int_0^{\infty} \left(\boldsymbol{\xi}^T \mathbf{Q} \boldsymbol{\xi} + \mathbf{v}^T \mathbf{R} \mathbf{v} \right) \mathrm{d}\lambda \\ \text{s.t.} \quad & \frac{\mathrm{d}\boldsymbol{\xi}}{\mathrm{d}\lambda} = \mathbf{A} \boldsymbol{\xi} + \mathbf{B} \mathbf{v}, \end{aligned} \tag{28}$$

where $\mathbf{Q} \geq \mathbf{0}$ and $\mathbf{R} > \mathbf{0}$. The structure of $\mathbf{Q}$ is specified as $\mathbf{Q} = \mathrm{diag}(q_1, q_2, q_3, q_4, q_5, q_6)$, with $q_3 = q_4$ and $q_5 = q_6$, so as to appropriately weight the equinoctial variable errors. Indeed, this results in

$$\begin{aligned} q_3 \, \xi_3^2 + q_4 \, \xi_4^2 &= q_3[(x_3 - x_3^*)^2 + (x_4 - x_4^*)^2] \\ q_5 \, \xi_5^2 + q_6 \, \xi_6^2 &= q_5[(x_5 - x_5^*)^2 + (x_6 - x_6^*)^2]. \end{aligned} \tag{29}$$

The solution to (28) is the standard LQR state feedback

$$\mathbf{v} = -\mathbf{K} \boldsymbol{\xi}, \tag{30}$$

where $\mathbf{K} = \mathbf{R}^{-1}\mathbf{B}^T\mathbf{P}$, and the positive definite matrix $\mathbf{P}$ is obtained by solving the continuous time algebraic Riccati equation $\mathbf{A}^T\mathbf{P} + \mathbf{P}\mathbf{A} - \mathbf{P}\mathbf{B}\mathbf{R}^{-1}\mathbf{B}^T\mathbf{P} + \mathbf{Q} = \mathbf{0}$. Note that radial thrusting can be excluded, if needed, by removing the first column of $\mathbf{B}$ in (28), since system (24) is still controllable when $v_1 = 0$. In particular, it is known that enforcing $v_1 = 0$ can actually result in an improved fuel efficiency, as discussed in [7, 30, 31].

B. Elliptical Case

In the elliptical orbit case, the control design procedure is more involved due to the time-varying nature of the linearized model (20). In order to obtain a closed-form solution, system (20) is approximated by a discrete-time model and a periodic LQR problem is cast as explained below.

Let $\{p_k\}_{k\in\mathbb{N}}$ be the sequence of equally spaced samples

$$p_k = \frac{2\pi(k-1)}{n} \tag{31}$$

of the true longitude, along the target orbit, where n is the number of samples per orbital revolution. The sequence $\{p_k\}_{k\in\mathbb{N}}$ corresponds to a sequence of mean longitudes $\{\lambda_k\}_{k\in\mathbb{N}}$, where λ_k is obtained by computing L according to (7) with $x_1 = p_k$, $x_3 = x_3^*$ and $x_4 = x_4^*$, i.e., $\lambda_k = L(p_k, x_3^*, x_4^*)$. Moreover, let us set

$$\lambda_{k+1} - \lambda_k = \Delta_k, \tag{32}$$

and observe that $\Delta_k > 0$ is a non-uniform sampling interval in the λ domain.

By choosing a sufficiently large number of samples n in (31), one can achieve $\Delta_k \ll 2\pi$ in (32). Under such condition, matrices $\mathbf{A}(\lambda)$ and $\mathbf{B}(\lambda)$ in (21)-(22) are approximately constant over one sampling interval Δ_k. Hence, a discretized version of system (20) can be obtained using the following zero-order hold equivalent

$$\boldsymbol{\xi}_{k+1} = \mathbf{A}_k \boldsymbol{\xi}_k + \mathbf{B}_k \mathbf{v}_k, \tag{33}$$

where

$$\mathbf{A}_k = e^{\mathbf{A}(\lambda_k)\Delta_k}$$

$$\mathbf{B}_k = \left(\int_0^{\Delta_k} e^{\mathbf{A}(\lambda_k)s}\mathrm{d}s\right)\mathbf{B}(\lambda_k).$$

Since $\mathbf{A}_k = \mathbf{A}_{k+n}$ and $\mathbf{B}_k = \mathbf{B}_{k+n}$ for all $k \in \mathbb{N}$, system (33) is periodic with period n in the discrete time index k.

The considered LQR problem is formulated as follows

$$\min_{\{\mathbf{v}_k\}} \ \sum_{k=1}^{\infty} \boldsymbol{\xi}_k^T \mathbf{Q}_k \boldsymbol{\xi}_k + \mathbf{v}_k^T \mathbf{R}_k \mathbf{v}_k \tag{34}$$

$$\text{s.t.} \ \ \boldsymbol{\xi}_{k+1} = \mathbf{A}_k \boldsymbol{\xi}_k + \mathbf{B}_k \mathbf{v}_k,$$

where $\mathbf{Q}_k = \mathbf{Q}\Delta_k$, $\mathbf{R}_k = \mathbf{R}\,\Delta_k$, and the performance index approximates the continuous quadratic cost in (28). The solution to (34) is [32]

$$\mathbf{v}_k = -\mathbf{K}_k \, \boldsymbol{\xi}_k, \tag{35}$$

where

$$\mathbf{K}_k = (\mathbf{B}_k^T \mathbf{P}_{k+1} \mathbf{B}_k + \mathbf{R}_k)^{-1} \mathbf{B}_k^T \mathbf{P}_{k+1} \mathbf{A}_k, \tag{36}$$

$\mathbf{K}_k = \mathbf{K}_{k+n}$, and the positive definite matrices $\mathbf{P}_k = \mathbf{P}_{k+n}$ are found by solving the periodic algebraic Riccati equation

$$\mathbf{P}_k = \mathbf{A}_k \mathbf{P}_{k+1} \mathbf{A}_k - \mathbf{A}_k^T \mathbf{P}_{k+1} \mathbf{B}_k (\mathbf{R}_k + \mathbf{B}_k^T \mathbf{P}_{k+1} \mathbf{B}_k)^{-1} \mathbf{B}_k^T \mathbf{P}_{k+1} \mathbf{A}_k + \mathbf{Q}_k \tag{37}$$

with $k = 1, \ldots, n$ and $\mathbf{P}_{n+1} = \mathbf{P}_1$. Note that (37) can be rewritten in compact form as follows

$$\bar{\mathbf{P}} = \bar{\mathbf{A}}^T \bar{\mathbf{P}} \bar{\mathbf{A}} - \bar{\mathbf{A}}^T \bar{\mathbf{P}} \bar{\mathbf{B}} (\bar{\mathbf{R}} + \bar{\mathbf{B}}^T \bar{\mathbf{P}} \bar{\mathbf{B}})^{-1} \bar{\mathbf{B}}^T \bar{\mathbf{P}} \bar{\mathbf{A}} + \bar{\mathbf{Q}}, \tag{38}$$

where

$$\bar{\mathbf{A}} = \begin{bmatrix} 0 & \cdots & \cdots & \mathbf{A}_n \\ \mathbf{A}_1 & 0 & \cdots & 0 \\ \vdots & \ddots & \vdots & \vdots \\ 0 & \cdots & \mathbf{A}_{n-1} & 0 \end{bmatrix}, \quad \bar{\mathbf{B}} = \begin{bmatrix} \mathbf{B}_n & \cdots & \cdots & 0 \\ 0 & \mathbf{B}_1 & \cdots & 0 \\ \vdots & \vdots & \ddots & \vdots \\ 0 & \cdots & \cdots & \mathbf{B}_{n-1} \end{bmatrix},$$

$\bar{\mathbf{P}} = \text{blockdiag}(\mathbf{P}_1, \ldots, \mathbf{P}_n)$, $\bar{\mathbf{Q}} = \text{blockdiag}(\mathbf{Q}_1, \ldots, \mathbf{Q}_n)$, and $\bar{\mathbf{R}} = \text{blockdiag}(\mathbf{R}_n, \mathbf{R}_1 \ldots, \mathbf{R}_{n-1})$.

To accommodate for variations of λ and $\boldsymbol{\xi}$ during the inter-sample period, a continuous control

law of the form

$$\mathbf{v} = -\mathbf{K}(\lambda)\,\boldsymbol{\xi} \tag{39}$$

can be reconstructed from (35) through linear interpolation, with

$$\mathbf{K}(\lambda) = \mathbf{K}_k + \frac{\lambda \bmod 2\pi - \lambda_k}{\Delta_k}(\mathbf{K}_{k+1} - \mathbf{K}_k), \qquad \lambda_k \le \lambda \bmod 2\pi \le \lambda_{k+1}.$$

Equation (39) describes a family of periodic controllers indexed by ϕ (see (19)). By enforcing $\phi = \xi_1$ in (19) and (39), i.e., by using the actual mean longitude error ξ_1 to select the controller within the family (39), a nonlinear regulator of the form

$$\mathbf{v} = -\mathbf{K}(L^* + \xi_1)\,\boldsymbol{\xi} \tag{40}$$

can be finally derived. Such a solution typically requires the parameter ϕ to vary slowly [33] (recall that ϕ is kept frozen in the linearization process). In our case, $d\phi/d\lambda = d\xi_1/d\lambda$ and this requirement is met as long as the error term ξ_2 and the control input $\mathbf{v}$ are small (see (20)-(22)).

The following remarks are in order:

(i) The use of a non-uniform sampling interval in (32) allows one to reduce the number of samples n required for an accurate discretization of system (20).

(ii) For a sufficiently large n in (31), the control law (39) approaches the infinite-horizon solution to the continuous-time, periodic LQR problem.

(iii) Since (38) is still solvable when the first column of $\mathbf{B}_k$ is removed, radial thrusting can be excluded.

(iv) For any nonzero target eccentricity e^*, one can specify the reference frame $\mathcal{F}$ (see Appendix A) as the perifocal frame of the target. In this way, the control gain in (40) can be made independent of x_4^* (it depends on this parameter via (23)).

The applicability of the proposed design is investigated in the next section.

V. Application to Orbit Phasing

In this section, the performance of the state-feedback controllers (30) and (40) is evaluated through numerical simulations on two representative orbit phasing maneuvers, featuring a circular and an elliptical orbit, respectively. The simulations are carried out by adopting a nonlinear truth model based on Cowell's formulation, accounting for perturbations due to the first nine harmonics of the Earth's geopotential, and for the control acceleration $\mathbf{u}$. It is assumed that both the chaser and the target are affected by gravitational perturbations. The short-periodic oscillations due to the $J2$ harmonic are removed from the tracking error by using Brouwer's transformation [34]. This corresponds to feeding back mean orbital elements, instead of osculating ones. The differential effect of secular gravitational perturbations is treated as an exogenous disturbance to be rejected by the control system. The control acceleration $\mathbf{u}$ is recovered from the input signal $\mathbf{v}$ by using (14).

A. Circular Orbit

Let us consider a circular coplanar rendezvous mission. The initial conditions of the chaser and the target spacecraft are reported in Table 1, in terms of mean orbital elements. These correspond to an orbital altitude of 800 km, and to a large initial inter-satellite separation (approximately 14000 km). To rendezvous, the chaser must perform an orbit phasing maneuver using only tangential thrust (this is feasible in the considered scenario). To this aim, the first and the third column of $\mathbf{B}$, as well as the state components ξ_5, ξ_6, are removed from (28), and the problem is solved by using the control input v_2 alone. The LQR matrices are set to $\mathbf{Q} = \mathrm{diag}(0.01, 50, 20, 20)$ and $\mathbf{R} = 5 \cdot 10^7$. The settling time for the maneuver is defined as the time required for the mean longitude error ξ_1

Table 1. Initial conditions (circular orbit)

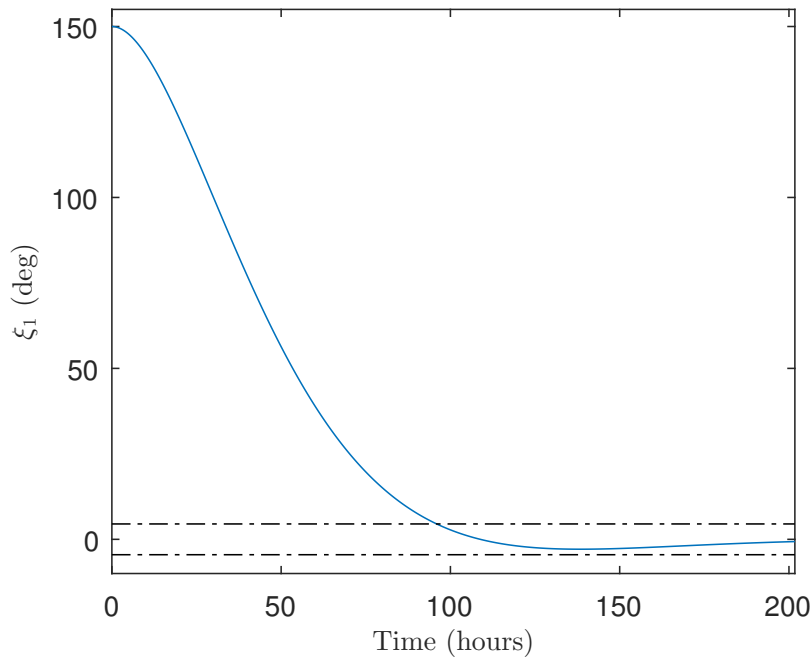| Equinoctial variable	Chaser	Target
True longitude	$x_1(0) = 150$ deg	$x_1^*(0) = 0$ deg
Mean motion	$x_2(0) = 0.001$ rad/s	$x_2^* = 0.001$ rad/s
Eccentricity vector	$x_3(0) = 0$	$x_3^* = 0$
	$x_4(0) = 0$	$x_4^* = 0$

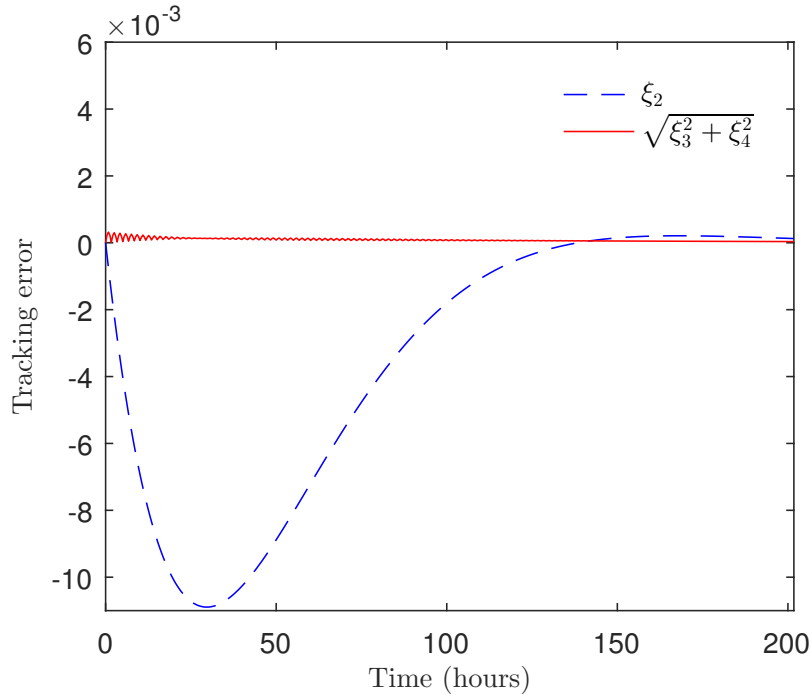**Figure 1. Mean longitude error profile and ±4.5 deg error band (circular orbit)**

Figure 2. Error variables ξ_2 and $\sqrt{\xi_3^2 + \xi_4^2}$ (circular orbit).

to reach and stay within 3% of its initial value (i.e., 4.5 deg).

The maneuver is simulated for 200 hours, corresponding to 120 orbital revolutions. The resulting mean longitude error is reported in Fig. 1 and converges to zero asymptotically, incurring a
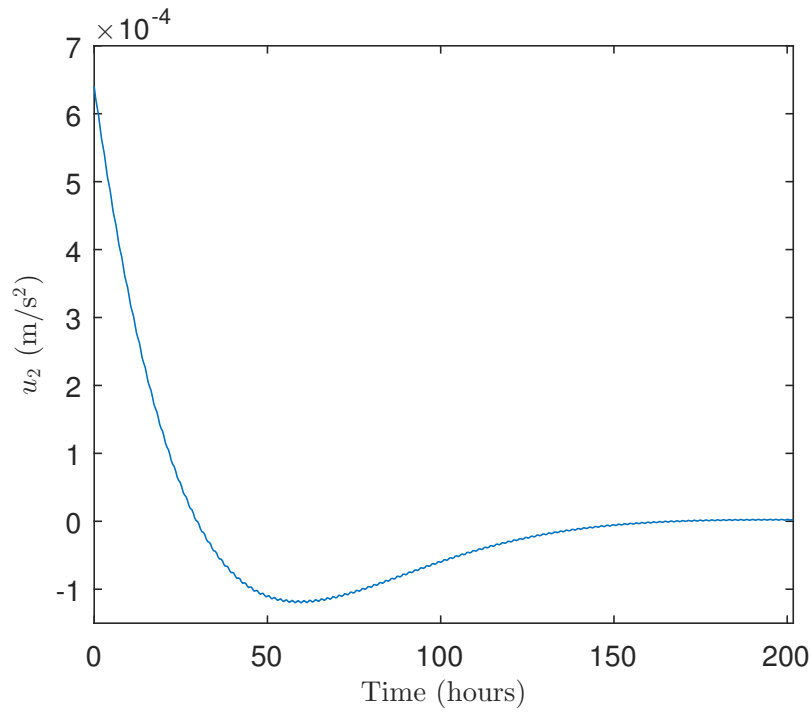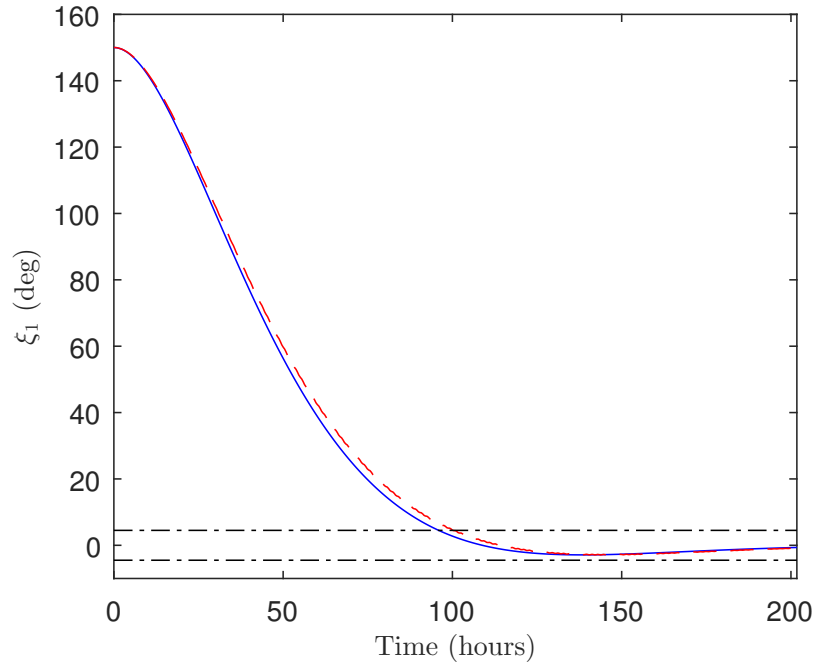
Figure 3. Control input u_2 (circular orbit).

Figure 4. Mean longitude error profiles obtained with the proposed design (solid) and with an HCW-based LQR using curvilinear coordinates (dashed): the two profiles are almost undistinguishable.

minor overshoot. The settling time is about 100 hours. The evolution of the error variables ξ_2 and $\sqrt{\xi_3^2 + \xi_4^2}$, see (12) and (29), is depicted in Fig. 2. It can be seen that the rendezvous objective is achieved satisfactorily, despite the large initial separation. The control acceleration u_2 is reported

in Fig. 3 and is compatible with the thrust per unit mass delivered by modern low-thrust engines (which is in the order of 10^{-4} m/s^2 [3]). The delta-v required by the maneuver amounts to approximately 52 m/s. A two-impulse phasing maneuver lasting 100 hours would require a delta-v of approximately 35 m/s, which is 30% lower than that of our design. This is explained by the fact that the cost function in (28) weights the control energy rather than the total delta-v.

It is worth noticing that the LTI system (24)-(25) takes on a form similar to that of the HCW equations, expressed in a curvilinear coordinate system [25]. In view of this analogy, it is expected for the design in Sec. IV.A to match the performance of an LQR control scheme based on the curvilinear HCW model. This is confirmed by Fig. 4, where the mean longitude error profiles obtained with the two controllers are displayed, for the case study considered above.

B.   Elliptical Orbit

Consider now a controlled spacecraft flown in an elliptic orbit similar to a Geostationary-Transfer-Orbit or a Molniya orbit, with a semi-major axis equal to 26500 km and an eccentricity of 0.7. The orbital inclination must be corrected by 3 degrees and the spacecraft must by re-phased by 160 deg in the mean longitude. By denoting the controlled spacecraft as the chaser and assuming a virtual leader, the maneuvering problem can be cast into the considered rendezvous setting. The initial conditions of the two satellites are reported in Table 2. The number of samples in (31) is set to $n = 100$.

The maneuver is simulated numerically by using the control law (40) tuned with $\mathbf{Q} = \mathrm{diag}(0.005, 5, 5, 5, 1, 1)$ and $\mathbf{R} = \mathrm{diag}(10^5, 10^5, 10^3)$. The tracking error signals resulting

Table 2. Initial conditions (elliptical orbit)

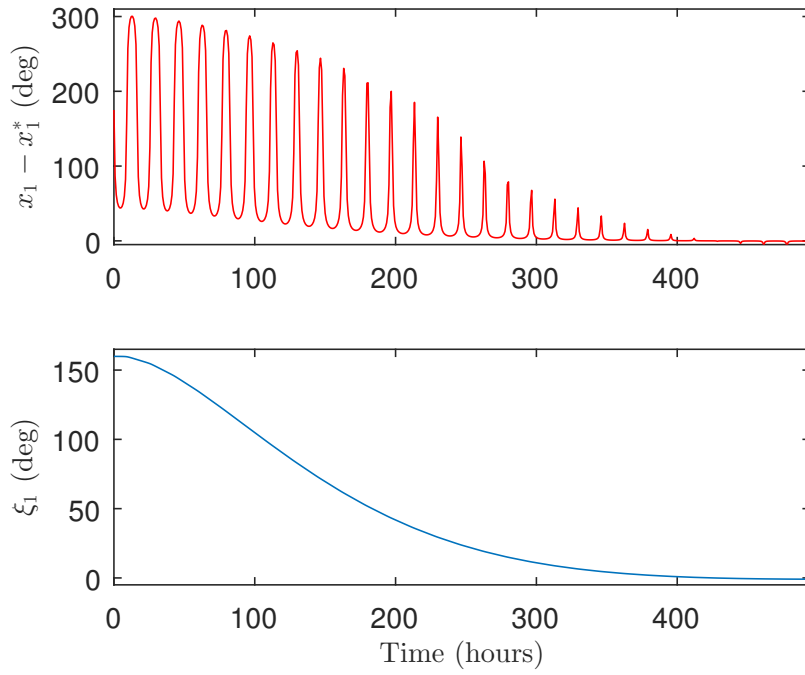| Equinoctial variable	Chaser	Target
True longitude	$x_1(0) = 175$ deg	$x_1^*(0) = 0$ deg
Mean motion	$x_2(0) = 0.00015$ rad/s	$x_2^* = 0.00015$ rad/s
Eccentricity vector	$x_3(0) = 0.7$	$x_3^* = 0.7$
	$x_4(0) = 0$	$x_4^* = 0$
Inclination vector	$x_5(0) = 0.0262$	$x_5^* = 0$
	$x_6(0) = 0$	$x_6^* = 0$

Figure 5. True longitude error $x_1 - x_1^*$ and mean longitude error ξ_1 (elliptical orbit).
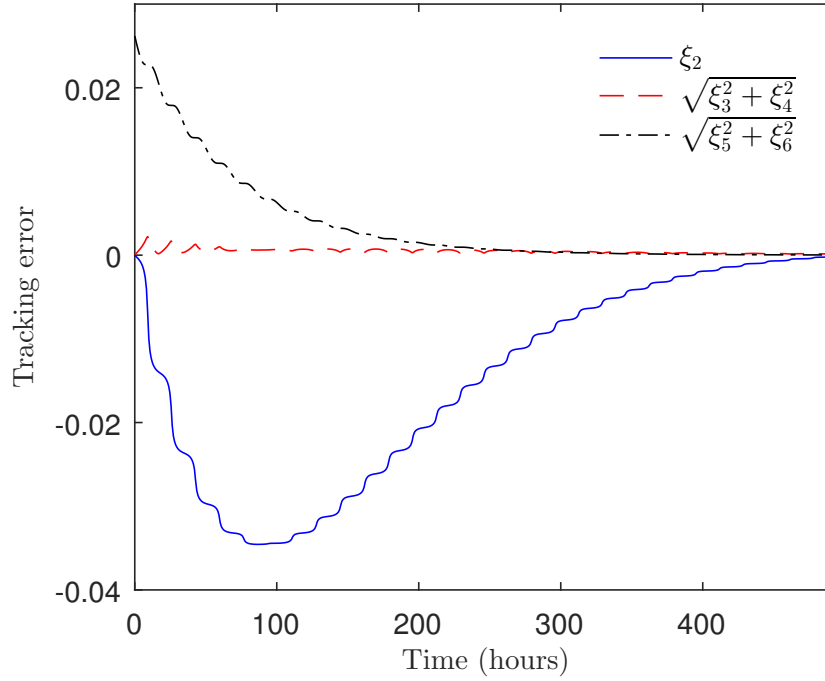

Figure 6. Error variables ξ_2, $\sqrt{\xi_3^2 + \xi_4^2}$ and $\sqrt{\xi_5^2 + \xi_6^2}$ (elliptical orbit).

from the simulation are reported in Figs. 5 and 6. Similarly to what observed for the circular case, the control objective is achieved satisfactorily, despite the large initial inter-satellite separation (approximately 65230 km). The oscillations of the true longitude error $x_1 - x_1^*$ in Fig. 5 are due to the
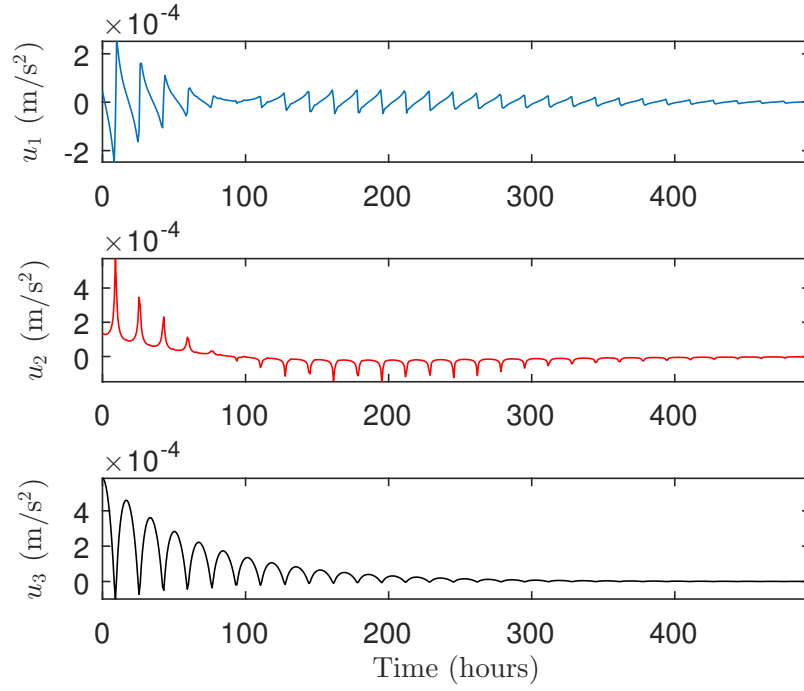
Figure 7. Control input u (elliptical orbit).
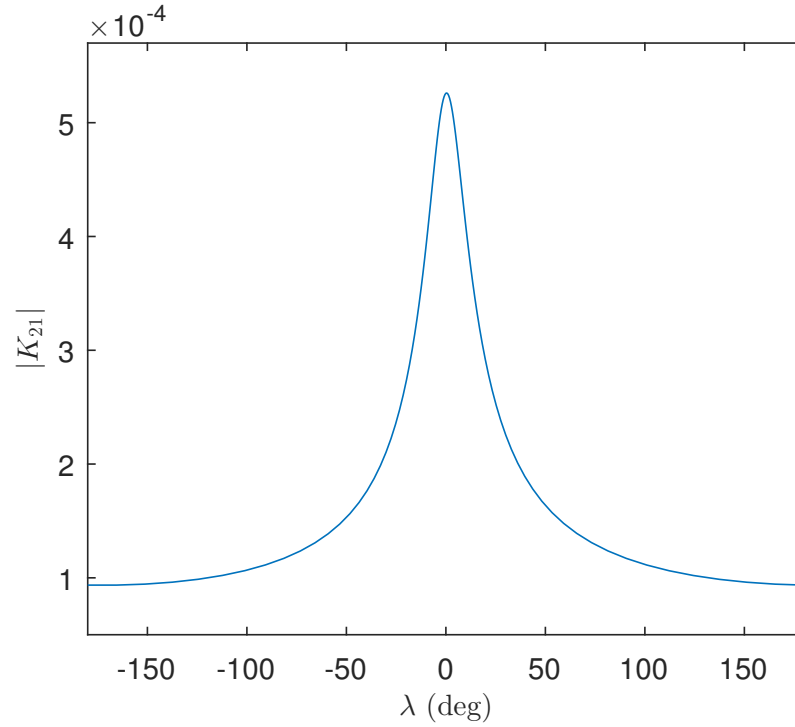
Figure 8. Profile of $|K_{21}(\lambda)|$.

natural dynamics of the formation, which moves along a highly elliptical orbit. In particular, the

positive peaks observed from $t = 200$ hours onwards occur when the two spacecraft pass close to

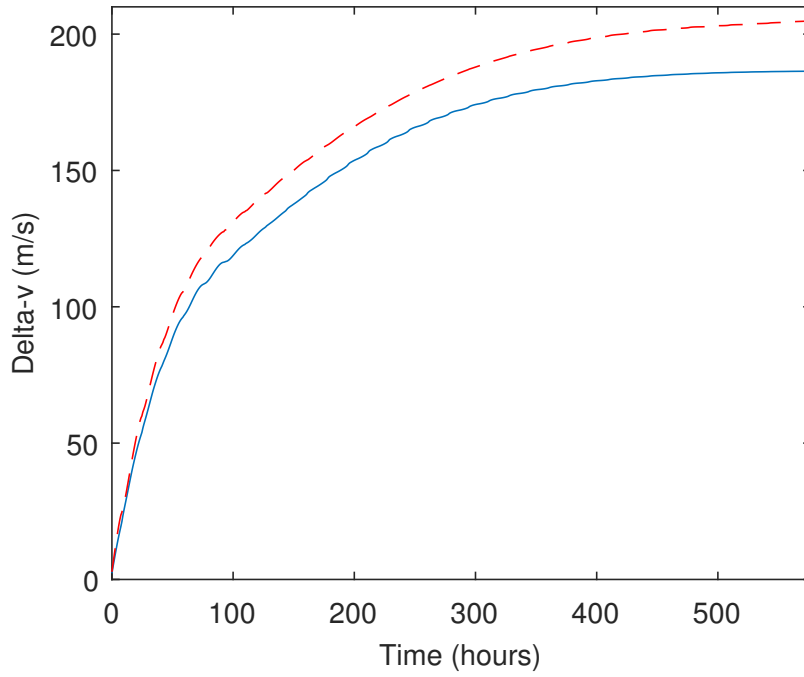the periapsis, where $x_1 - x_1^*$ can be large even for a small mean longitude (i.e., phase) error ξ_1. This

Figure 9. **Maneuver delta-v: controller** (30) **(dashed), and controller** (40) **(solid).**

is precisely the reason why the mean longitude error ξ_1 is used instead of the true longitude error, in the feedback scheme proposed in this work.

The control acceleration **u**, resulting from the simulation, is reported in Fig. 7. It can be noticed that its magnitude is compatible with low-thrust propulsion systems. The spikes in the control signals are due to the time-varying gain matrix $\mathbf{K}(\lambda)$, which promotes corrections of specific orbital elements at specific points of the orbit (note that the simulation covers 30 orbital periods). In particular, it is interesting to analyze the profile of the second entry in the first column of $\mathbf{K}(\lambda)$, which represents the control gain from the mean longitude error ξ_1 to the control input v_2. The absolute value of this gain, reported in Fig. 8, is maximal at the chaser periapsis ($\lambda = 0$, see (39)-(40) and Table 2). This is in line with physical intuition, since the time derivative of the mean motion error ξ_2 is more sensitive to v_2 at this point (see (22)-(23)), and ξ_1 can be controlled by suitably varying ξ_2 (see (21)).

The performance of the controller (40) has been compared to that of the LQR feedback law (30) designed on the time-invariant model (24). It is observed that (30) can still stabilize the nonlinear plant. As expected, (40) provides a higher fuel efficiency (see Fig. 9, which reports the total delta-v for the maneuver). Finally, it is worth remarking that the HCW-based LQR presented in Section

fails to stabilize the considered elliptical reference.

VI.   Conclusions

By using equinoctial variables, we derived a family of linearized models describing the relative motion between two satellites located at different angular positions, within a given orbit. These models have been exploited to design two linear quadratic regulators solving the phasing control problem. The results of numerical simulations indicate that the controller performance is adequate for space missions involving low-thrust maneuvers, in both circular and elliptical orbits.

Appendix

A.   Reference frame $\mathcal{F}$

The inertial reference frame $\mathcal{F}$ adopted in this paper coincides with the equinoctial coordinate system (EQW, see [1]) defined by the (unperturbed) target orbit, as illustrated in Fig. 10. Let the vectors $\mathbf{z}(t) \in \mathbb{R}^6$ and $\mathbf{z}^*(t) \in \mathbb{R}^6$ describe the position and velocity of the chaser and the target, respectively, in the Earth-Centered-Inertial (ECI) frame. Moreover, let $\mathbf{C}(\cdot)$ be the direction cosine matrix which transforms the ECI frame to the EQW frame and $\mathbf{\Phi}(\cdot)$ be the mapping from cartesian coordinates to the orbital elements (1). The orbital elements of the chaser and the target,
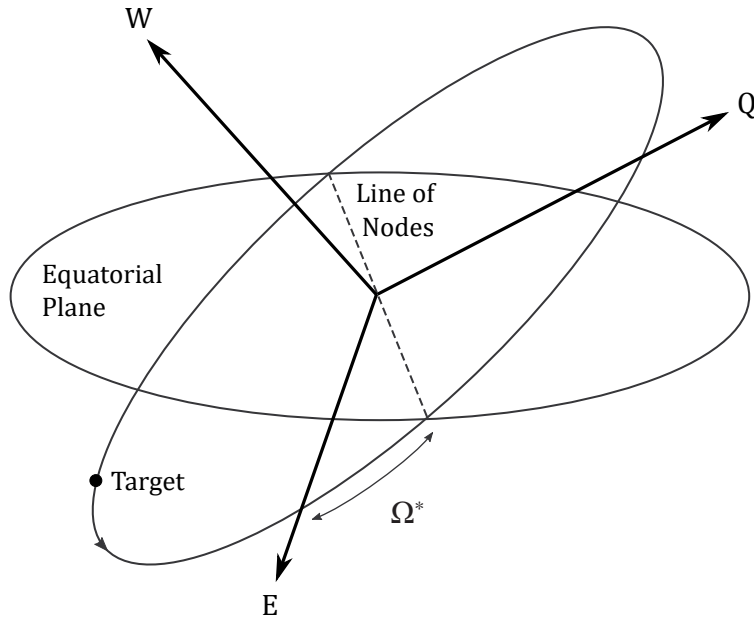

Figure 10. EQW frame.

expressed with respect to $\mathcal{F}$, are given by $\mathbf{x}(t) = \boldsymbol{\Phi}(\boldsymbol{\Lambda}\mathbf{z}(t))$ and $\mathbf{x}^*(t) = \boldsymbol{\Phi}(\boldsymbol{\Lambda}\mathbf{z}^*(t))$, respectively, where $\boldsymbol{\Lambda} = \text{blockdiag}(\mathbf{C}(\mathbf{z}^*(0)), \mathbf{C}(\mathbf{z}^*(0)))$. Notice that in frame $\mathcal{F}$ the nominal value of the target inclination is 0 by definition.

References

[1] Vallado, D. A., *Fundamentals of Astrodynamics and Applications*, Springer-Verlag New York, 3rd ed., 2007.

[2] Starek, J. A., Açıkmeşe, B., Nesnas, I. A., and Pavone, M., "Spacecraft Autonomy Challenges for Next-Generation Space Missions," *Advances in Control System Technology for Aerospace Applications*, Springer, 2016, pp. 1–48. doi:10.1007/978-3-662-47694-9_1.

[3] Leomanni, M., Garulli, A., Giannitrapani, A., and Scortecci, F., "Propulsion Options for Very Low Earth Orbit Microsatellites," *Acta Astronautica*, Vol. 133, 2017, pp. 444–454. doi:10.1016/j.actaastro.2016.11.001.

[4] Clohessy, W. H. and Wiltshire, R. S., "Terminal Guidance System for Satellite Rendezvous," *Journal of Aerospace Sciences*, Vol. 27, No. 9, 1960, pp. 653–658. doi:10.2514/8.8704.

[5] Hempel, P. and Tschauner, J., "Rendezvous with a Target in an Elliptical Orbit," *Acta Astronautica*, Vol. 11, No. 2, 1965, pp. 104–109.

[6] Ulybyshev, Y., "Long-term Formation Keeping of Satellite Constellation Using Linear-Quadratic Controller," *Journal of Guidance, Control, and Dynamics*, Vol. 21, No. 1, 1998, pp. 109–115. doi:doi.org/10.2514/2.4204.

[7] Starin, S. R., Yedavalli, R., and Sparks, A. G., "Spacecraft Formation Flying Maneuvers Using Linear Quadratic Regulation with no Radial Axis Inputs," *AIAA Guidance, Navigation, and Control Conference and Exhibit*, Montreal, Canada, 2001, pp. 6–9. doi:10.2514/6.2001-4029.

[8] Gao, H., Yang, X., and Shi, P., "Multi-Objective Robust Control of Spacecraft Rendezvous," *IEEE Transactions on Control Systems Technology*, Vol. 17, No. 4, 2009, pp. 794–802. doi:10.1109/TCST.2008.2012166.

[9] Richards, A. and How, J. P., "Robust Variable Horizon Model Predictive Control for Vehicle Maneuvering," *International Journal of Robust and Nonlinear Control*, Vol. 16, No. 7, 2006, pp. 333–351. doi:10.1002/rnc.1059.

[10] Di Cairano, S., Park, H., and Kolmanovsky, I., "Model Predictive Control Approach for Guidance of Spacecraft Rendezvous and Proximity Maneuvering," *International Journal of Robust and Nonlinear Control*, Vol. 22, No. 12, 2012, pp. 1398–1427. doi:10.1002/rnc.2827.

[11] Leomanni, M., Rogers, E., and Gabriel, S. B., "Explicit Model Predictive Control Approach for Low-Thrust Spacecraft Proximity Operations," *Journal of Guidance, Control, and Dynamics*, Vol. 37, No. 6, 2014, pp. 1780–1790. doi:10.2514/1.G000477.

[12] Shibata, M. and Ichikawa, A., "Orbital Rendezvous and Flyaround based on Null Controllability with Vanishing Energy," *Journal of Guidance, Control, and Dynamics*, Vol. 30, No. 4, 2007, pp. 934–945. doi:10.2514/1.24171.

[13] Zhou, B., Lin, Z., and Duan, G.-R., "Lyapunov Differential Equation Approach to Elliptical Orbital Rendezvous with Constrained Controls," *Journal of Guidance, Control, and Dynamics*, Vol. 34, No. 2, 2011, pp. 345–358. doi:10.2514/1.52372.

[14] Lantoine, G. and Epenoy, R., "Quadratically Constrained Linear-Quadratic Regulator Approach for Finite-Thrust Orbital Rendezvous," *Journal of Guidance, Control, and Dynamics*, Vol. 35, No. 6, 2012, pp. 1787–1797. doi:10.2514/1.56961.

[15] Gao, X., Teo, K. L., and Duan, G.-R., "Robust H_∞ Control of Spacecraft Rendezvous on Elliptical Orbit," *Journal of the Franklin Institute*, Vol. 349, No. 8, 2012, pp. 2515–2529. doi:10.1016/j.jfranklin.2012.08.005.

[16] Hartley, E. N. and Maciejowski, J. M., "Field Programmable Gate Array Based Predictive Control System for Spacecraft Rendezvous in Elliptical Orbits," *Optimal Control Applications and Methods*, Vol. 36, No. 5, 2015, pp. 585–607. doi:10.1002/oca.2117.

[17] Vazquez, R., Gavilan, F., and Camacho, E. F., "Pulse-Width Predictive Control for LTV Systems with Application to Spacecraft Rendezvous," *Control Engineering Practice*, Vol. 60, 2017, pp. 199–210. doi:10.1016/j.conengprac.2016.06.017.

[18] Kellett, C. M. and Praly, L., "Nonlinear Control Tools for Low Thrust Orbital Transfer," *Proceedings of the 6th IFAC Symposium on Nonlinear Control Systems*, Stuttgart, Germany, 2004. doi:10.1016/S1474-6670(17)31203-X.

[19] Singla, P., Subbarao, K., and Junkins, J. L., "Adaptive Output Feedback Control for Spacecraft Rendezvous and Docking under Measurement Uncertainty," *Journal of Guidance, Control, and Dynamics*, Vol. 29, No. 4, 2006, pp. 892–902. doi:10.2514/1.17498.

[20] Leomanni, M., Bianchini, G., Garulli, A., and Giannitrapani, A., "A Class of Globally Stabilizing Feedback Controllers for the Orbital Rendezvous Problem," *International Journal of Robust and Nonlinear Control*, Vol. 27, No. 18, 2017, pp. 4607–4621. doi:10.1002/rnc.3817.

[21] Steindorf, L. M., D'Amico, S., Scharnagl, J., Kempf, F., and Schilling, K., "Constrained Low-Thrust Satellite Formation-Flying using Relative Orbit Elements," *27th AAS/AIAA Space Flight Mechanics Meeting*, San Antonio, US, 2017.

[22] Crassidis, J. L., Markley, F. L., Anthony, T. C., and Andrews, S. F., "Nonlinear Predictive Control of Spacecraft," *Journal of Guidance, Control, and Dynamics*, Vol. 20, No. 6, 1997, pp. 1096–1103. doi:10.2514/2.4191.

[23] Park, C., Guibout, V., and Scheeres, D. J., "Solving Optimal Continuous Thrust Rendezvous Problems with Generating Functions," *Journal of Guidance, Control, and Dynamics*, Vol. 29, No. 2, 2006, pp. 321–331. doi:10.2514/1.14580.

[24] Starek, J. A. and Kolmanovsky, I. V., "Nonlinear Model Predictive Control Strategy for Low Thrust Spacecraft Missions," *Optimal Control Applications and Methods*, Vol. 35, No. 1, 2014, pp. 1–20. doi:10.1002/oca.2049.

[25] Gill, E. and How, J., "Comparative Analysis of Cartesian and Curvilinear Clohessy-Wiltshire Equations," *Journal of Aerospace Engineering, Sciences and Applications*, Vol. 3, No. 2, 2011, pp. 1–15. doi:10.7446/jaesa.

[26] Kasdin, N. J., Gurfil, P., and Kolemen, E., "Canonical Modelling of Relative Spacecraft Motion via Epicyclic Orbital Elements," *Celestial Mechanics and Dynamical Astronomy*, Vol. 92, No. 4, 2005, pp. 337–370. doi:10.1007/s10569-004-6441-7.

[27] D'Amico, S. and Montenbruck, O., "Proximity Operations of Formation-Flying Spacecraft Using an Eccentricity/Inclination Vector Separation," *Journal of Guidance Control and Dynamics*, Vol. 29, No. 3, 2006, pp. 554–563. doi:10.2514/1.15114.

[28] Koenig, A. W., Guffanti, T., and D'Amico, S., "New State Transition Matrices for Spacecraft Relative Motion in Perturbed Orbits," *Journal of Guidance, Control, and Dynamics*, Vol. 40, No. 7, 2017, pp. 1749–1768. doi:10.2514/1.G002409.

[29] Battin, R. H., *An Introduction to the Mathematics and Methods of Astrodynamics*, American Institute of Aeronautics and Astronautics, Inc., Reston, Virginia, 1999.

[30] Riggi, L. and D'Amico, S., "Optimal Impulsive Closed-Form Control for Spacecraft Formation Flying and Rendezvous," *American Control Conference*, Boston, US, 2016, pp. 5854–5861. doi:10.1109/ACC.2016.7526587.

[31] Chernick, M. and D'Amico, S., "New Closed-form Solutions for Optimal Impulsive Control of Spacecraft Relative Motion," *Journal of Guidance, Control, and Dynamics*, Vol. 41, No. 2, 2017, pp. 301–319. doi:10.2514/1.G002848.

[32] Bittanti, S. and Colaneri, P., *Periodic Systems: Filtering and Control*, Springer-Verlag London, 2009. doi:10.1007/978-1-84800-911-0.

[33] Cimen, T., "Survey of State-Dependent Riccati Equation in Nonlinear Optimal Feedback Control Synthesis," *Journal of Guidance, Control and Dynamics*, Vol. 35, No. 4, 2012, pp. 1025–1047. doi:10.2514/1.55821.

[34] Brouwer, D., "Solution of the Problem of Artificial Satellite Theory Without Drag," *The Astronomical Journal*, Vol. 64, 1959, pp. 378–397. doi:10.1086/107958.